Ab initio study of the electron-phonon coupling at the Cr(001) surface

L. Peters,[1,*] A. N. Rudenko,[2,3,1] and M. I. Katsnelson[1,3]

[1]*Institute for Molecules and Materials, Radboud University Nijmegen, NL-6525 AJ Nijmegen, The Netherlands*
[2]*School of Physics and Technology, Wuhan University, Wuhan 430072, China*
[3]*Theoretical Physics and Applied Mathematics Department, Ural Federal University, 620002 Ekaterinburg, Russia*

It is experimentally well established that the Cr(001) surface exhibits a sharp resonance around the Fermi level. However, there is no consensus about its physical origin. It is proposed to be either due to a single particle d_{z^2} surface state renormalized by electron-phonon coupling or the orbital Kondo effect involving the degenerate d_{xz}/d_{yz} states. In this paper we examine the electron-phonon coupling of the Cr(001) surface by means of *ab-initio* calculations in the form of density functional perturbation theory. More precisely, the electron-phonon mass-enhancement factor of the surface layer is investigated for the 3d states. For the majority and minority spin d_{z^2} surface states we find values of 0.19 and 0.16. We show that these calculated electron-phonon mass-enhancement factors are not in agreement with the experimental data even if we use realistic values for the temperature range and surface Debye frequency for the fit of the experimental data. More precisely, then experimentally an electron-phonon mass-enhancement factor of 0.70 ± 0.10 is obtained, which is not in agreement with our calculated values of 0.19 and 0.16. Our findings suggest that the experimentally observed resonance at the Cr(001) surface is not due to electron-phonon effects but due to electron-electron correlation effects.

I. INTRODUCTION

The electrode-electrolyte interface in a battery, topological insulators, multilayer devices, and at contacts are examples where surface physics plays an important role. In the field of spintronics magnetic multilayers are used to exploit the different tunneling probabilities of the spin-up and spin-down electrons for the development of novel devices. For this purpose a thorough understanding of the physical mechanisms behind the tunneling process is required [1,2]. For example, in chromium magnetic multilayers it is known that complicated many-body effects at the surface are responsible for the tunneling [3].

Surface physics is also fundamentally very interesting due to the occurrence of new and unexpected features. For example, for the Cr(001) surface a sharp resonance close to the Fermi level is observed in angular resolved photoemission and scanning tunneling experiments [4–7]. Another reason for the large interest in chromium is its peculiar magnetic properties. Its magnetic ground state is described by a spin-density wave with a long period modulating the amplitude of the magnetic moments along the $\langle 001 \rangle$ direction, which is incommensurate with the underlying body centered cubic structure [8].

In order to understand the physical origin of the observed resonance at the Fermi level several experimental and theoretical investigations were conducted. The first idea was to explain the resonance in terms of a single particle d_{z^2} surface state [7,9]. A shortcoming of this idea was the unrealistic reduction of the magnetic moment required to obtain the correct resonance position. Another interpretation in terms

of an orbital Kondo effect involving the degenerate d_{xz} and d_{yz} states was proposed to explain the scanning tunneling spectroscopy experiments on very clean Cr(001) surfaces [10,11]. Then, scanning tunneling spectroscopy experiments were performed in a wide temperature range [12]. It was observed that the experimental data could be explained both in terms of the d_{z^2} surface state and orbital Kondo effect. Although for the former an electron-phonon coupling strength 5–10 times larger than in the bulk had to be assumed. On the other hand the orbital Kondo effect was called into question by a combination of scanning tunneling spectroscopy, photoemission spectroscopy, and inverse photoemission spectroscopy experiments [13]. It was demonstrated that the resonance above the Fermi level was mainly of d_{z^2} character. However, it should be realized that the resolution of inverse photoemission spectroscopy is not sufficient to be conclusive about the character of the sharp resonance emerging at low temperatures.

In the newest experiments a different behavior is observed than in the earlier experiments [14]. Namely a pseudogap is found below roughly 200 K and the emergence of a sharp resonance below 75 K. These observations hint in the direction of a many-body interpretation of the resonance just as recent dynamical mean-field theory (DMFT) calculations do [15,16]. For example, based on DMFT calculations within the continuous-time quantum Monte Carlo (CTQMC) solver it was observed that the resonance was very robust against artificial shifts in the one-particle energies of the d_{xz}, d_{yz}, and d_{z^2} states. In contrast for DMFT calculations based on the spin-polarized T-matrix fluctuation exchange approximation, which is suitable for weakly and moderately correlated systems, no resonance was observed. However, the high-energy features, everything except the resonance, of the spectrum were

*L.Peters@science.ru.nl

successfully explained within this method. Finally, the non-crossing approximation (NCA) was employed within DMFT, which is basically designed to capture (orbital) Kondo-like processes. Depending on the starting point, it was observed that an orbital Kondo resonance might evolve in the presence of a strong magnetic field like in the Cr(001) surface. This could not be verified due to spurious behavior involved with the spin-polarized version of the NCA method [16,17].

In this paper it is investigated whether the d_{z^2} surface state renormalized by means of the electron-phonon coupling is responsible for the experimentally observed resonance at the Fermi level of Cr(001) surfaces. More precisely, the electron-phonon mass-enhancement factor of the Cr(001) surface is investigated and a comparison is made with that of the bulk by means of *ab initio* calculations. For this purpose a linear response scheme in terms of the density functional perturbation theory (DFPT) within a pseudopotential plane-wave approach is employed [18–20]. We first tested this method on paramagnetic and antiferromagnetic Cr-bulk and found electron-phonon mass-enhancement factors in reasonable agreement with strong-coupling theory and good agreement with optical pump-and-probe experiment, respectively [21,22]. For the Cr(001) surface we obtained for the majority and minority spin d_{z^2} surface states electron-phonon mass-enhancement factors of, respectively, 0.19 and 0.16. We show that these calculated values are not in agreement with the experimental data even if we use realistic values for the temperature range and surface Debye frequency for the fit of the experimental data. More precisely, then experimentally an electron-phonon mass-enhancement factor of 0.70 ± 0.10 is obtained, which is not in agreement with our calculated values of 0.19 and 0.16. Our findings suggest that the experimentally observed resonance at the Cr(001) surface is not due to electron-phonon effects but due to electron-electron correlation effects. More studies are needed to exactly determine which many-body processes are responsible for the resonance.

The rest of the paper is organized as follows. The method and computational details are presented in Sec. II. Section III contains the results and discussion, and finally in Sec. IV we conclude.

II. METHOD AND COMPUTATIONAL DETAILS

The response of an electron system to external perturbations is commonly studied in physics. An efficient and accurate technique to do this is density-functional perturbation theory (DFPT), which is a combination of density-functional theory (DFT) and linear response theory [18,19,23,24]. For example, this method allows the investigation of the coupling between the electrons and phonons in a system. It is known that many physical properties are determined by this coupling, e.g., electrical and thermal conductivity, and superconductivity.

DFT is based on the fact that the total energy of an interacting electron system is a functional of the electron density and the variational principle [23]. In order to obtain the ground state of the interacting electron system in general a mapping to a set of single-particle equations is

performed [24],

$$\hat{H}_{\text{DFT}}\psi_{\mathbf{k}\nu} = \left(\frac{\hat{\mathbf{p}}^2}{2m} + V_{\text{eff}}[n]\right)\psi_{\mathbf{k}\nu} = \epsilon_{\mathbf{k}\nu}\psi_{\mathbf{k}\nu},$$

$$V_{\text{eff}}[n] = V_{\text{ion}}[n] + V_H[n] + V_{xc}[n]. \tag{1}$$

Here the first term between brackets is the kinetic energy operator. The $\psi_{\mathbf{k}\nu}$ and $\epsilon_{\mathbf{k}\nu}$ are the so-called Kohn-Sham eigenstates and eigenenergies. Further, V_{eff} is the effective potential which is a functional of the electron density. This functional can be separated into three parts: the interaction of the electrons with the ions (V_{ion}), a Hartree term (V_H), and exchange-correlation part (V_{xc}). The latter contains the exchange and correlation effects among the electrons. For this part the functional dependence on the density is not exactly known and approximations are used in practice. The most popular approximations are derived in the limit of a (nearly) uniform electron gas, i.e., the local density approximation (LDA) and the generalized gradient approximation (GGA) [25–27]. Then, by using the following expression for the electron density,

$$n(\mathbf{r}) = \sum_{\mathbf{k}\nu} f_{\mathbf{k}\nu}|\psi_{\mathbf{k}\nu}|^2, \tag{2}$$

the system can be solved self-consistently. Here, $f_{\mathbf{k}\nu}$ corresponds to the occupation number of the state $\psi_{\mathbf{k}\nu}$.

After obtaining the self-consistent solution of Eqs. (1) and (2), linear response theory can be used to investigate the coupling of the phonon and electron systems. For this purpose the displacement pattern corresponding to a phonon is considered as a static perturbation for the electron system within DFPT, i.e., the Born-Oppenheimer approximation. As can be inferred from Eq. (1) a perturbation will lead to a change of the electron density Δn and effective potential ΔV_{eff}, which within linear response can be obtained self-consistently from the following set of equations

$$\Delta n = 4Re\sum_{\mathbf{k}\nu}^{\text{occ}} \psi_{\mathbf{k}\nu}^*\Delta\psi_{\mathbf{k}\nu},$$

$$(\hat{H}_{\text{DFT}} - \epsilon_{\mathbf{k}\nu})\Delta\psi_{\mathbf{k}\nu} = -(\Delta V_{\text{eff}} - \Delta\epsilon_{\mathbf{k}\nu})\psi_{\mathbf{k}\nu},$$

$$\Delta V_{\text{eff}} = \Delta V_{\text{ion}} + \frac{1}{2}\int\frac{\Delta n(\mathbf{r}')}{|\mathbf{r} - \mathbf{r}'|}d\mathbf{r}' + \frac{dV_{xc}}{dn}\bigg|_n\Delta n. \tag{3}$$

Here the tag *occ* above the summation correponds to a summation over occupied states only and $\Delta\epsilon_{\mathbf{k}\nu} = \langle\psi_{\mathbf{k}\nu}|\Delta V_{\text{eff}}|\psi_{\mathbf{k}\nu}\rangle$ is the first-order variation of the Kohn-Sham eigenvalue.

After the set of equations in Eq. (3) has been solved self-consistently for the atomic perturbations, phonon and electron-phonon coupling related quantities can be calculated. For example, with the Hellman-Feynman theorem it can be shown that from the linear response of the density Δn the dynamical matrix can be constructed from which the phonon frequencies and modes can be computed. Further, from the first-order derivative of the self-consistent Kohn-Sham potential ΔV_{eff} the electron-phonon coupling matrix elements can be

obtained

$$g_{\mathbf{k+q,k}}^{\mathbf{q}j,\nu\mu} = \left(\frac{\hbar}{2\omega_{\mathbf{q}j}}\right)^{1/2} \langle\psi_{\mathbf{k+q}\mu}|\Delta V_{\mathrm{eff}}^{\mathbf{q}j}|\psi_{\mathbf{k}\nu}\rangle, \qquad (4)$$

where $\omega_{\mathbf{q}j}$ refers to the phonon frequency corresponding to the phonon mode with wave vector $\mathbf{q}$ and index j. From these electron-phonon coupling matrix elements and the phonon frequencies important quantities can be determined such as the spectral function (isotropic Eliashberg function) $\alpha^2 F(\omega)$ and the isotropic coupling constant (electron-phonon mass-enhancement factor) λ,

$$\alpha^2 F(\omega) = \frac{1}{N(\epsilon_F)} \sum_{\mu\nu} \sum_{\mathbf{q}j} \delta(\omega - \omega_{\mathbf{q}j}) \sum_{\mathbf{k}} \left|g_{\mathbf{k+q,k}}^{\mathbf{q}j,\nu\mu}\right|^2$$
$$\times \delta(\epsilon_{\mathbf{k+q}\mu} - \epsilon_F)\delta(\epsilon_{\mathbf{k}\nu} - \epsilon_F),$$
$$\lambda = 2\int \frac{\alpha^2 F(\omega)}{\omega} d\omega. \qquad (5)$$

Here $N(\epsilon_F)$ is the density of states at the Fermi level indicated by ϵ_F.

From temperature dependent scanning tunneling spectroscopy experiments on the Cr(001)-surface an electron-phonon mass-enhancement factor 5–10 times larger than in the bulk is predicted [12]. This prediction is obtained under the assumption that the resonance at the Fermi level is due to a d_{z^2}-surface state renormalized by electron-phonon coupling. Thus, this predicted λ corresponds to the d_{z^2} state of the surface layer. However, computationally a Cr(001) surface is simulated by a finite number of layers. Then, the λ calculated from Eq. (5) corresponds in general to the whole system, i.e., not specifically to the top layer. Therefore, a projection is required to obtain λ corresponding to the top layer and d_{z^2} state. In principle one could argue that a surface layer projection could be obtained by a consideration of the surface phonon modes only. Namely, it might be expected that the electronic surface states couple the strongest to surface phonon modes. However, we investigated this and found that the electronic surface states couple the strongest to phonons involving vibrations in all the layers. Therefore, in order to obtain a proper projection it is instructive to first consider the $\psi_{\mathbf{k}\nu}$ dependence of the spectral function explicitly

$$\alpha^2 F_{\mathbf{k}\nu}(\omega) = \sum_{\mu} \sum_{\mathbf{q}j} \delta(\omega - \omega_{\mathbf{q}j})\left|g_{\mathbf{k+q,k}}^{\mathbf{q}j,\nu\mu}\right|^2 \delta(\epsilon_{\mathbf{k+q}\mu} - \epsilon_F). \quad (6)$$

Here $\alpha^2 F(\omega)$ of Eq. (5) is obtained by performing the following average over the Fermi surface $\alpha^2 F(\omega) = \frac{1}{N(\epsilon_F)} \sum_{\mathbf{k}\nu} \alpha^2 F_{\mathbf{k}\nu}(\omega)\delta(\epsilon_{\mathbf{k}\nu} - \epsilon_F)$. The projection of the $\alpha^2 \widehat{F}(\omega)$ operator onto the local basis $|\mathbf{R}\xi\rangle$ (with $\mathbf{R}$ referring to the layer and $\xi = m\sigma$ containing both the orbital and spin projection) can be expressed in terms of Eq. (6) and the $\langle\mathbf{R}\xi|\mathbf{k}\nu\rangle$ coefficients,

$$\langle\mathbf{R}\xi|\alpha^2\widehat{F}(\omega)|\mathbf{R}'\xi'\rangle = \sum_{\mathbf{k}\nu} \langle\mathbf{R}\xi|\mathbf{k}\nu\rangle\alpha^2 F_{\mathbf{k}\nu}(\omega)\langle\mathbf{k}\nu|\mathbf{R}'\xi'\rangle, \quad (7)$$

where $\alpha^2 F_{\mathbf{k}\nu}(\omega) = \langle\mathbf{k}\nu|\alpha^2\widehat{F}(\omega)|\mathbf{k}\nu\rangle$. Then, by performing the appropriate summation and averaging over the Fermi surface

the $|\mathbf{R}\xi\rangle$ dependence of $\alpha^2 F(\omega)$ can be obtained

$$\alpha^2 F_{\mathbf{R}\xi}(\omega) = \frac{1}{N(\epsilon_F)_{\mathbf{R}\xi}} \sum_{\mathbf{R}'\xi'} \langle\mathbf{R}\xi|\alpha^2\widehat{F}(\omega)|\mathbf{R}'\xi'\rangle$$
$$\times \langle\mathbf{R}'\xi'|\delta(\hat{H}_{\mathrm{DFT}} - \epsilon_F)|\mathbf{R}\xi\rangle$$
$$= \frac{1}{N(\epsilon_F)_{\mathbf{R}\xi}} \sum_{\mathbf{k}\nu} \alpha^2 F_{\mathbf{k}\nu}(\omega)\delta(\epsilon_{\mathbf{k}\nu} - \epsilon_F)|\langle\mathbf{R}\xi|\mathbf{k}\nu\rangle|^2. \tag{8}$$

The expression in the last line of this equation is obtained by employing the unity operator $\sum_{\mathbf{k}\nu} |\mathbf{k}\nu\rangle\langle\mathbf{k}\nu|$ twice and inserting Eq. (7). Here $N(\epsilon_F)_{\mathbf{R}\xi}$ is the projected density of states at the Fermi energy at the site with position vector $\mathbf{R}$ and of the state indicated by $\xi = m\sigma$. Further, $\alpha^2 F(\omega)$ of Eq. (5) is obtained by performing the summation $\frac{1}{N(E_F)} \sum_{\mathbf{R}\xi} \alpha^2 F_{\mathbf{R}\xi}(\omega)N(\epsilon_F)_{\mathbf{R}\xi}$.

On its turn $\alpha^2 F_{\mathbf{R}\xi}(\omega)$ of Eq. (8) can used to calculate the $|\mathbf{R}\xi\rangle$ projected electron-phonon mass-enhancement factor $\lambda_{\mathbf{R}\xi}$ and averaged λ [of Eq. (5)] via

$$\lambda_{\mathbf{R}\xi} = 2\int \frac{\alpha^2 F_{\mathbf{R}\xi}(\omega)}{\omega} d\omega,$$
$$\lambda = \frac{1}{N(\epsilon_F)} \sum_{\mathbf{R}\xi} \lambda_{\mathbf{R}\xi} N(\epsilon_F)_{\mathbf{R}\xi}. \qquad (9)$$

The calculations in this work are performed by employing the DF(P)T implementation of the QUANTUM ESPRESSO code [28,29]. An ultrasoft pseudopotential is used to reduce the required plane-wave kinetic energy cutoff with respect to norm-conserving pseudopotentials [30,31]. For details on the DFPT implementation with ultrasoft pseudopotentials we refer the reader to Ref. [32]. Unless stated otherwise, the calculations are performed with an exchange-correlation functional in the generalized gradient approximation (GGA) as formulated by Perdew, Burke, and Ernzerhof (PBE) [27]. For the Cr(001)-surface calculations a kinetic energy cutoff for the expansion into plane waves of the wave functions and density of, respectively, 70 Ry and 800 Ry were taken. In case of Cr-bulk calculations 50 Ry and 600 Ry were used. It was tested that the relevant quantities in this work, e.g. the electron-phonon mass-enhancement factors, are converged with respect to these energy cutoffs.

From Eqs. (5) and (8) it can be seen that summations over electronic ($\mathbf{k}$) and phononic ($\mathbf{q}$) meshes are required. Since the electron-phonon coupling matrix elements are known to depend smoothly on $\mathbf{k}$ and $\mathbf{q}$, the interpolation scheme presented in Ref. [20] is adapted. For the Cr(001)-surface calculations we tested that for a $15 \times 15 \times 1$ to $30 \times 30 \times 1$ interpolation of the $\mathbf{k}$ mesh and $5 \times 5 \times 1$ to $10 \times 10 \times 1$ interpolation of the $\mathbf{q}$-mesh convergence of the quantities of interest is achieved. As for the Cr-bulk calculations an interpolation of the $\mathbf{k}$ mesh from $15 \times 15 \times 15$ to $30 \times 30 \times 30$ and for the $\mathbf{q}$ mesh from $5 \times 5 \times 5$ to $10 \times 10 \times 10$ was found to be adequate.

Further, the calculations were scalar relativistic and spin polarized, where an antiferromagnetic magnetic structure was taken. In addition for all DF(P)T calculations a geometry optimization is performed such that the total energy and forces are converged to within 10^{-5} Ry and 10^{-4} a.u. For the Cr(001)-surface calculations a large vacuum of at least

20 Å was introduced to prevent interactions between layers of different unit cells. The Cr-bulk simulations were for the bcc structure. After geometry optimization a lattice constant of 2.87 Å was obtained for an antiferromagnetic magnetic structure and 2.83 Å for the paramagnetic situation.

III. RESULTS AND DISCUSSION

Before the electron-phonon mass-enhancement factor of the Cr(001) surface is investigated, first the Cr bulk is addressed. In Table I the electron-phonon mass-enhancement factor (second column) and the density of states at the Fermi level ϵ_F per atom (third column) are presented for paramagnetic (PM) and antiferromagnetic (AFM) Cr bulk. Further, both the LDA and the GGA exchange-correlation functional were employed. Since within LDA no stable AFM state could be obtained, the electron-phonon mass-enhancement factor could not be determined. The lack of a stable AFM solution within LDA is also observed in other studies [9,33]. However, for the paramagnetic state the difference between LDA and GGA appears to be small. Furthermore, from this table a large suppression in λ of about a factor 3 can be observed for the antiferromagnetic structure compared to that of the paramagnetic case. Interestingly, this same factor also corresponds to the difference observed in the density of states at the Fermi level. Such a dependence of λ on the density of states at the Fermi level can be inferred from Eq. (6) by assuming that the electron-phonon matrix elements ($g_{\mathbf{k+q,k}}^{\mathbf{q}j,\nu\mu}$) are approximately constant and that the phonon energies ($\omega_{\mathbf{q}j}$) can be neglected with respect to the electronic energies. Then, the term $\sum_{\mathbf{q}\mu} \delta(\epsilon_{\mathbf{k+q}\mu} - \epsilon_F)$ gives the proportionality with the density of states at the Fermi level.

The suppression of superconductivity in the antiferromagnetic phase for Cr bulk is a known phenomenon [21]. Note that λ is the central quantity in superconducting theory. Further, our calculated value of λ for the antiferromagnetic phase is found to be in good agreement with optical pump-and-probe experiment, $\lambda = 0.13 \pm 0.02$ [21]. Unfortunately, the λ obtained for the paramagnetic phase cannot be compared with experiment. However, strong coupling theory predicted a λ of 0.25 for the paramagnetic phase, which is in reasonable agreement with our result [22]. It should be noted that the method we employed is much more sophisticated than strong coupling theory.

In the following the electron-phonon mass-enhancement factor of the Cr(001) surface is investigated. For this purpose it is instructive to first inspect the 3d projected density of states of the Cr(001) surface, i.e., the top layer of a system consisting of multiple layers. For this surface layer the total 3d

TABLE I. The electron-phonon mass-enhancement factor λ and density of states at the Fermi level per atom ϵ_F for paramagnetic (PM) and antiferromagnetic (AFM) Cr bulk are presented. Here LDA and GGA refer to the employed exchange-correlation functional.

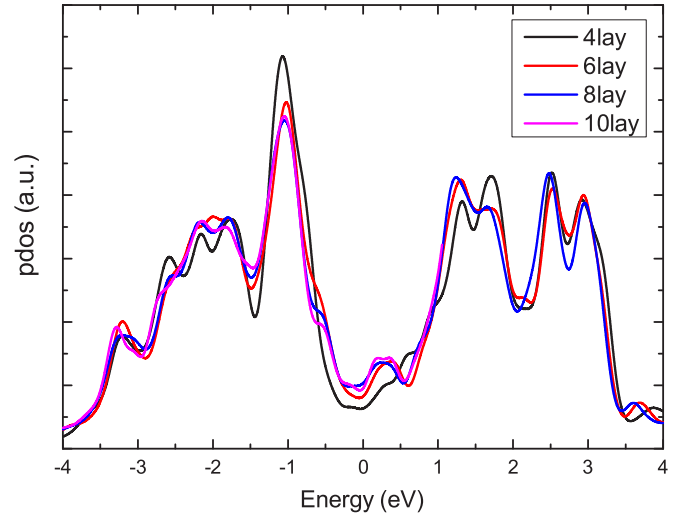|	λ	$N(\epsilon_F)$
PM (LDA)	0.37	4.7
PM (GGA)	0.35	4.8
AFM (GGA)	0.12	1.7

FIG. 1. The total 3d projected density of states of the surface layer for calculations in which different numbers of layers are considered. Here black corresponds to a calculation of four layers, red to six layers, blue to eight layers, and pink to ten layers.

projected density of states is depicted in Fig. 1 for calculations in which different numbers of layers are considered. Here black corresponds to a calculation of four layers, red to six layers, blue to eight layers, and pink to ten layers. From Fig. 1 it can be observed that for eight layers the projected density of states can be considered converged with respect to the total number of layers. Especially note that the important region for the electron-phonon mass-enhancement factor, which is around the Fermi level, is well converged for eight layers. Further, our computed 3d projected density of states is in good agreement with what is obtained in previous DFT studies [9,15]. In addition, in Ref. [9] a detailed analysis can be found of the orbital and layer projected band structure.

In Fig. 2 the electron-phonon mass-enhancement factor of Eq. (9) corresponding to the top layer and the different 3d states is presented for calculations of different numbers of layers. Here the top figure refers to the majority spin state and the bottom figure to the minority spin state. Further, black corresponds to d_{z^2}, red to d_{xz}/d_{yz} (are equivalent due to symmetry at the surface), blue to $d_{x^2-y^2}$, pink to d_{xy}, and green to the per spin averaged $\frac{1}{N(E_F)_{\mathbf{R}\sigma}} \sum_m \lambda_{\mathbf{R}m\sigma} N(\epsilon_F)_{\mathbf{R}\xi}$, where $\mathbf{R}\xi = \mathbf{R}m\sigma$, m is the sum over the different 3d states, and $N(E_F)_{\mathbf{R}\sigma}$ is the spin-projected and layer-projected density of states at the Fermi level. From this figure it can be observed that for all majority spin 3d states the electron-phonon mass-enhancement factor appears to be quite well converged with respect to the number of layers. For the minority spin 3d states the fluctuation as function of the number of layers is a bit larger. This is especially the case for the d_{xz}/d_{yz} states. However, the important observation is that for the (majority and minority) d_{z^2} surface state the electron-phonon mass-enhancement factor seems to be converged already for six layers. Therefore, we consider 0.19 and 0.16 to be the electron-phonon mass-enhancement factor for, respectively, the majority and minority d_{z^2} surface state of the Cr(001) surface.
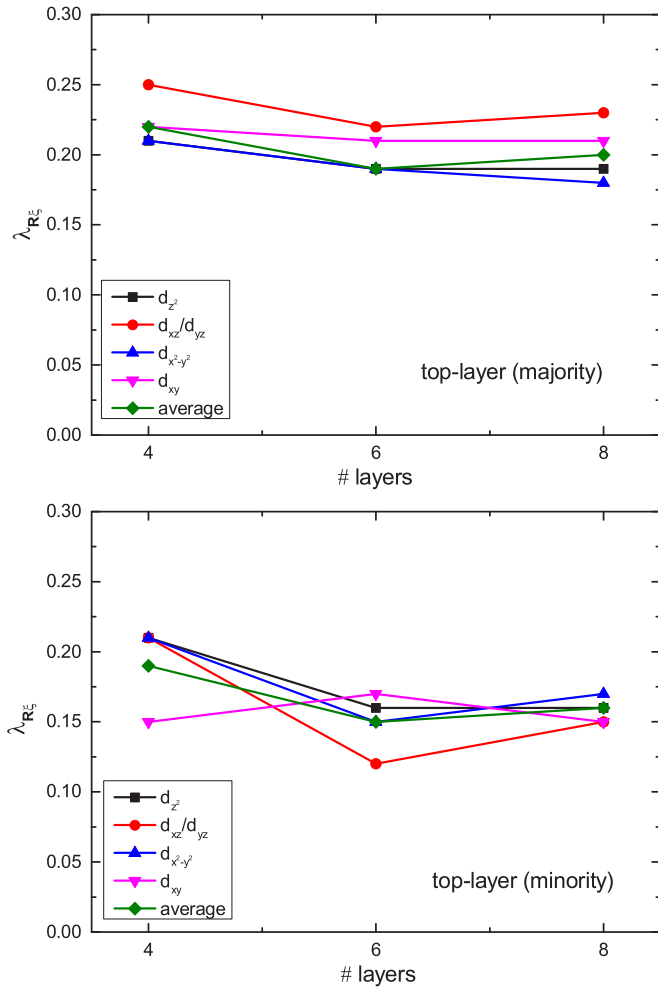
FIG. 2. The electron-phonon mass-enhancement factor of Eq. (9) corresponding to the top layer and the different 3d states is presented for calculations of different numbers of layers. Here the top figure refers to the majority spin states and the bottom figure to the minority spin states. Further, black corresponds to d_{z^2}, red to d_{xz}/d_{yz}, blue to $d_{x^2-y^2}$, pink to d_{xy}, and green to the spin averaged $\frac{1}{N(\epsilon_F)_{\mathbf{R}\sigma}} \sum_m \lambda_{\mathbf{R}m\sigma} N(\epsilon_F)_{\mathbf{R}\xi}$, where $\mathbf{R}\xi = \mathbf{R}m\sigma$, m is the sum over the different 3d states and $N(E_F)_{\mathbf{R}\sigma}$ is the spin-projected and layer-projected density of states at the Fermi level.
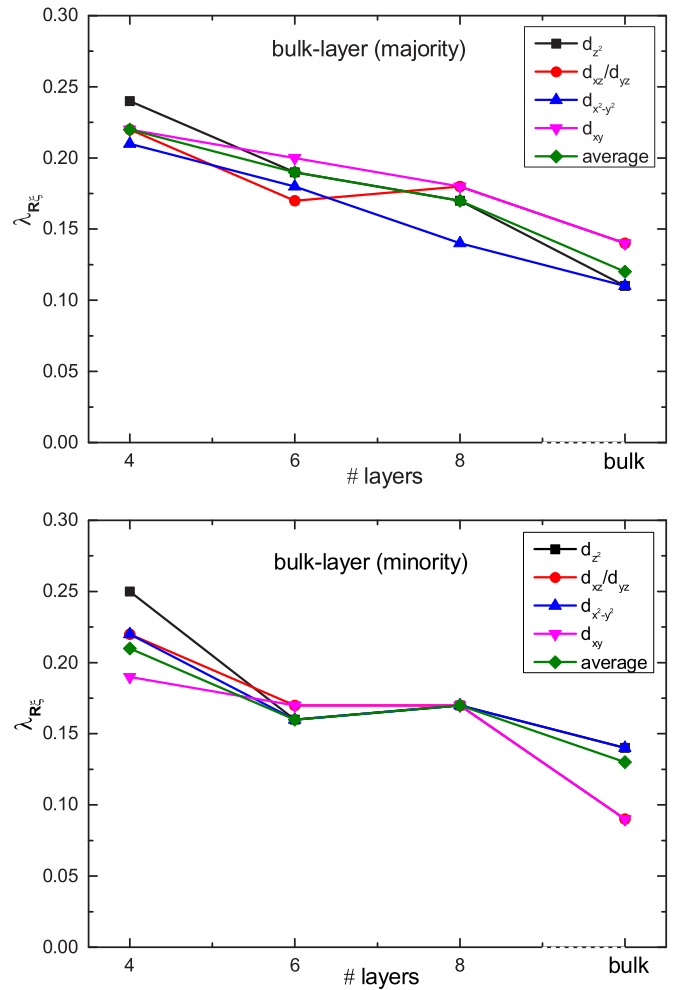
FIG. 3. The electron-phonon mass-enhancement factor of Eq. (9) corresponding to the bulk layer (middle layer) and the different 3d states is presented for calculations of different numbers of layers. Here the top figure refers to the majority spin states and the bottom figure to the minority spin states. Further, black corresponds to d_{z^2}, red to d_{xz}/d_{yz}, blue to $d_{x^2-y^2}$, pink to d_{xy}, and green to the spin averaged $\frac{1}{N(E_F)_{\mathbf{R}\sigma}} \sum_m \lambda_{\mathbf{R}m\sigma} N(\epsilon_F)_{\mathbf{R}\xi}$, where $\mathbf{R}\xi = \mathbf{R}m\sigma$, m is the sum over the different 3d states, and $N(E_F)_{\mathbf{R}\sigma}$ is the spin-projected and layer-projected density of states at the Fermi level.

A further inspection of Fig. 2 shows that on average the electron-phonon mass-enhancement factor for the majority 3d states is a bit larger than for the minority 3d states. The largest electron-phonon mass-enhancement factor is obtained for the d_{xz}/d_{yz} majority states, while the smallest for the d_{xz}/d_{yz} minority states.

It is also interesting to investigate the electron-phonon mass-enhancement factor of the 3d states corresponding to the bulk layer (middle layer). This is presented in Fig. 3, where results for the Cr bulk (indicated by 'bulk') are also included. Note that for Cr bulk due to symmetry the d_{z^2} and $d_{x^2-y^2}$ states are equivalent, and also the d_{xz}, d_{yz}, and d_{xy} states. Therefore, for these states the electron-phonon mass-enhancement factors should become equivalent as the number of layers increases. For eight layers the majority d_{xz}, d_{yz}, and d_{xy} states are equivalent, even though the bulk value is not reached. This

also occurs for the minority d_{xz}, d_{yz}, and d_{xy} states, and d_{z^2} and $d_{x^2-y^2}$ states. That the bulklike values are not achieved for eight layers can be partly explained by the fact that the projected density of states at the Fermi level is not converged with respect to the number of layers. As a typical example, the d_{z^2} projected density of states of the bulk layer is presented as a function of the number of layers in Fig. 4. From this figure it is clear that for ten layers the projected density of states around the Fermi level is not converged with respect to the number of layers.

As mentioned above the main interest is the electron-phonon mass-enhancement factor of the d_{z^2} state corresponding to the top layer. It was found that this quantity is converged already for six layers, which is in contrast to what was obtained for the bulk layer. Therefore, the electron-phonon mass-enhancement factors of the majority and minority d_{z^2}
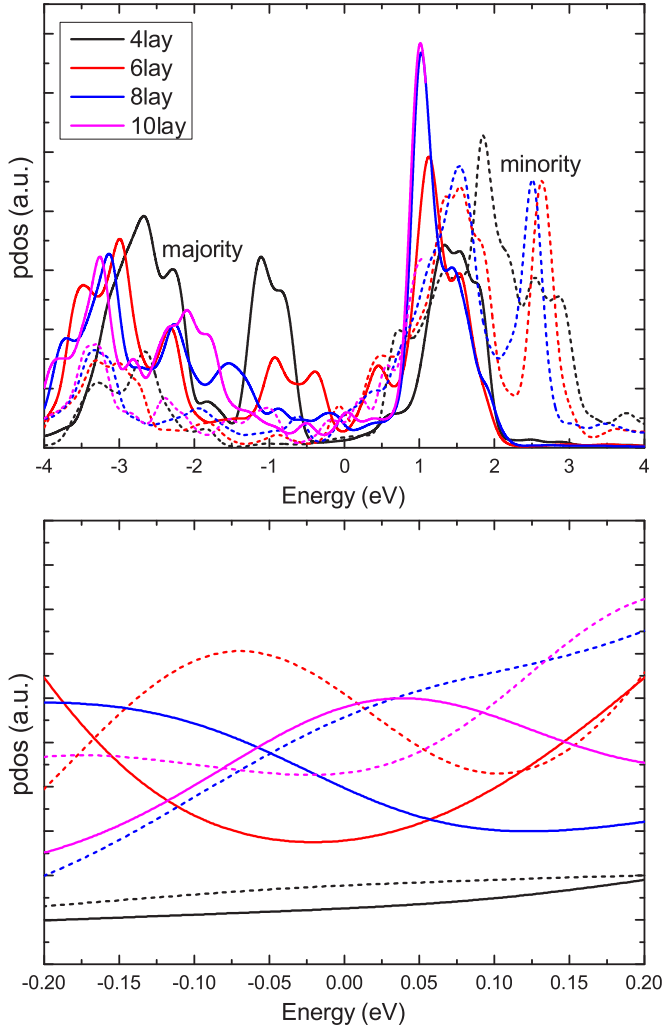
FIG. 4. The d_{z^2} projected density of states of the bulk layer (middle layer) for calculations in which different numbers of layers are considered. Here black corresponds to a calculation of four layers, red to six layers, blue to eight layers, and pink to ten layers. The solid lines refer to the majority spin channel and the dashed lines to the minority spin channel. The bottom figure is a zoom-in of the top figure around the Fermi level.

surface states, 0.19 and 0.16, are compared directly to those corresponding to the bulk of 0.11 and 0.14. There is less than a factor 2 difference between them. The same holds when a comparison is made with the bulk spin averaged electron-phonon mass-enhancement factors of 0.12 and 0.13. On the other hand, experimentally a factor of about 5–10 was predicted. For convenience, the values of 0.19 and 0.16 can also be directly compared with the absolute value predicted in experiment, 1.53 ± 0.40 [12]. It is clear that none of our calculated values are in agreement with this prediction.

It should be noted that the mismatch with experiment is smaller, when realistic values for the temperature range and surface Debye frequency are employed for the fit of the experimental data. In order to understand this, the procedure to obtain the electron-phonon mass-enhancement factor in Ref. [12] has to be inspected more closely. In their work the

experimental data is fitted with the following model,

$$\Gamma_{e-ph}(T) = \Gamma_{ee} + \lambda_{\mathrm{sur}} \frac{2\pi}{\omega_D^2} \int_0^{\omega_D} dE' E'^2 [1 - f(E_0 - E')$$
$$+ 2n(E') + f(E_0 + E')]. \tag{10}$$

Here ω_D is the Debye frequency corresponding to the surface, T the temperature, λ_{sur} is the electron-phonon mass-enhancement factor of the d_{z^2}-surface state, E_0 is the position of the resonance, $f(E)$ the Fermi distribution, and $n(E)$ the Bose-Einstein distribution. Further, Γ_{e-ph} is the inverse lifetime due to electron-phonon processes within the Debye model, and Γ_{ee} is the inverse lifetime due to the electron-electron interactions. The latter can be approximated by a constant for energies close to the Fermi level and low enough temperatures, i.e., it then corresponds to the offset observed at zero temperature.

The first thing we noticed is that in Ref. [12] λ_{sur} is assumed to be constant, while the model of Eq. (10) is used to fit the data in a temperature range of 4–350 K. The problem is that in this temperature range the paramagnetic to antiferromagnetic phase transition is crossed at 311 K. From for example Table I it is clear that the electron-phonon mass-enhancement factor can change drastically between these regimes. Therefore, we performed a fitting in the temperature range 4–178 K with Eq. (10) to obtain Γ_{ee}, λ_{sur}, and ω_D, where we took $E_0 = 20 \pm 5$ meV (same as in Ref. [12]). It appears then that the error bars of the experimental data are too large to accurately predict these quantities, $\Gamma_{ee} = 14 \pm 9$, $\lambda_{\mathrm{sur}} = 1.50 \pm 1$, and $\omega_D = 48 \pm 25$. This is the reason why in Ref. [12] (and also in Ref. [34]) only two quantities are fitted at a time and for the other a 'reasonable' guess is taken. More precisely, in Ref. [12] first the Debye frequency ω_D corresponding to the surface is taken to be equal to the bulk, 52.5 meV, for the determination of Γ_{ee} and λ. However, for the Cr(001) surface the Debye frequency has been found both experimentally and theoretically to be at least two times smaller than in the bulk [35,36]. On the other hand, $\Gamma_{ee} = 19.5 \pm 5$ meV seems to be a reasonable approximation for the offset observed at zero temperature in Fig. 3(b) of Ref. [12]. Then, taking $\omega_D = 26$ meV (half of the bulk value) and $\Gamma_{ee} = 19.5 \pm 5$ meV (and $E_0 = 20 \pm 5$ meV) we find for λ_{sur} by employing Eq. (10) in the temperature range 4–178 K the following, $\lambda_{\mathrm{sur}} = 0.77 \pm 0.16$. It is clear that this value is not in agreement with the calculated electron-phonon mass-enhancement factors of the majority and minority spin surface d_{z^2} states (0.19 and 0.16).

We could also use $\Gamma_{ee} = 19.5 \pm 5$ meV and $E_0 = 20 \pm 5$ meV to find both λ_{sur} and ω_D (corresponding to the surface) by employing Eq. (10) in the temperature range 4–178 K. Then, $\lambda = 1.44 \pm 0.83$ and $\omega_D = 48 \pm 25$ are found. From these results it appears again that the error bars of the experimental data points are too large to accurately determine these quantities. Therefore, we are convinced that it is better to take $\omega_D = 16$ meV from experiment [35]. Then, employing Eq. (10) with $\Gamma_{ee} = 19.5 \pm 5$ meV and $E_0 = 20 \pm 5$ meV in a temperature range of 4–178 K results in $\lambda_{\mathrm{sur}} = 0.70 \pm 0.10$, which is not in agreement with our calculations.

It is instructive to verify whether the Debye model can be employed to fit the experimental data. This can be conveniently done by an inspection of the Eliashberg function of Eq. (8). Therefore, the Eliashberg function corresponding to the top
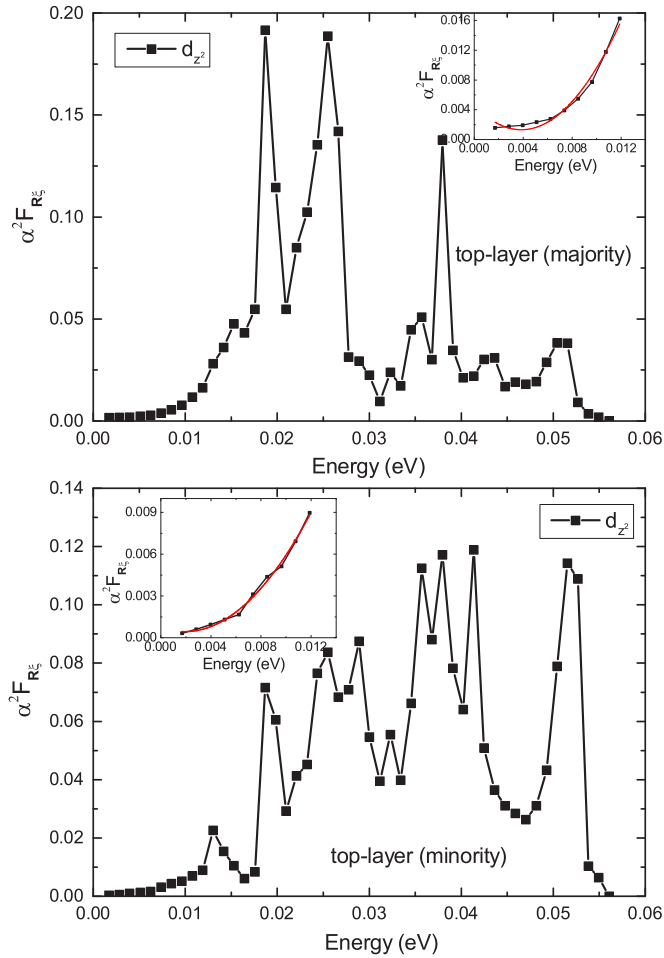
FIG. 5. For an eight layer calculation the Eliashberg function of Eq. (8) corresponding to the top layer and d_{z^2} state is presented for the majority (top) and minority (bottom) spin states. Further, in the inset graphs the red line corresponds to a second order polynomial fit, i.e., the Debye model.

layer and the d_{z^2} state is presented in Fig. 5. Here the top figure corresponds to the majority spin state and the bottom figure to the minority spin state. Further, in the inset graphs the red line corresponds to a second order polynomial fit, the Debye model, of the low energy frequencies. From these inset graphs it can be observed that for the majority spin state the agreement with the Debye model is reasonable, and for the minority spin state it is very good. Therefore, we are convinced that a fit by means of the Debye model is appropriate for the experimental data.

Besides the difference of about a factor 3 between our calculations and the experimental prediction, there is a subtlety that should be addressed in more detail. This subtlety is related with the interpretation of the experimentally observed resonance at the Fermi level of Cr(001) surfaces in terms of a d_{z^2}-surface state renormalized by electron-phonon coupling. Namely in absence of the electron-phonon coupling, i.e., at zero temperature, there should still be a peak at the Fermi level with a width determined by electron-electron interactions (Γ_{ee}) and impurities. However, from our DFT calculations it is clear that there is no such d_{z^2} peak in the vicinity of the Fermi level

(see the bottom figure of Fig. 1). The closest peak is at about 0.2 eV with a width of roughly 0.25 eV. This position is too far from the Fermi level and the width too large for the peak to allow for a substantial renormalization by electron-phonon coupling. For a substantial renormalization by means of the electron-phonon coupling it is known that both the position (with respect to the Fermi level) and the width of the peak can be at most of the order of the Debye frequency [37]. In an earlier work it was proposed that the overestimation of the magnetic moment within DFT was responsible for the wrong peak position [9]. However, it was immediately found that a correct peak position would result in an unrealistic underestimation of the magnetic moment [9]. In addition, the too large width of the peak could not be resolved by this. Another reason for the lack of a d_{z^2} peak with a correct width at the Fermi level could be an insufficient treatment of electron-electron correlation effects. In recent DFT+DMFT calculations within the CTQMC solver, it has been demonstrated that depending on the double counting a d_{z^2} peak can emerge at the Fermi level (see Fig. 3(d) of Ref. [15]).

IV. CONCLUSION

We have performed density functional perturbation theory calculations within a pseudopotential plane-wave approach to investigate the electron-phonon mass-enhancement factor of Cr(001) surfaces and Cr bulk. For Cr bulk we made the interesting observation that within the paramagnetic phase the electron-phonon mass-enhancement factor is about three times larger than in the antiferromagnetic phase. The same difference is found in the density of states at the Fermi level, which explains this behavior. Further, for the antiferromagnetic phase the calculated electron-phonon mass-enhancement factor is found to be in good agreement with experiment, while for the paramagnetic phase a reasonable agreement with strong coupling theory is obtained. For the paramagnetic phase it was also found that there is only a small difference between the electron-phonon mass-enhancement factor obtained in LDA and GGA.

For the Cr(001) surface we obtained for the majority and minority spin d_{z^2} surface states an electron-phonon mass-enhancement factor of, respectively, 0.19 and 0.16. Compared to the bulk these are less than a factor 2 larger, while experimentally a factor 5–10 difference was predicted. Further, we showed that the difference between experiment and our calculations is smaller if we use realistic values for the temperature range and surface Debye frequency to fit the experimental data. More precisely, then experimentally an electron-phonon mass-enhancement factor of 0.70 ± 0.10 is obtained, which is not in agreement with our calculated values of 0.19 and 0.16.

These findings suggest that the experimentally observed sharp resonance at the Fermi level of the Cr(001) surface is not due to electron-phonon effects, i.e., is not due to a d_{z^2} surface state renormalized by electron-phonon coupling. Instead, electron-electron correlations effects are expected to be responsible for the occurrence of the resonance. However, more studies are needed to exclude the importance of electron-phonon coupling effects beyond the Eliashberg theory and to investigate the effect of the electron-electron related many-body processes.

ACKNOWLEDGMENTS

[1] J. Sólyom and A. Zawadowski, Phys. Kondens. Mater. **7**, 325 (1968).

[2] A. Zawadowski, Phys. Rev. **163**, 341 (1967).

[3] P. LeClair, J. T. Kohlhepp, H. J. M. Swagten, and W. J. M. de Jonge, Phys. Rev. Lett. **86**, 1066 (2001).

[4] L. E. Klebanoff, S. W. Robey, G. Liu, and D. A. Shirley, Phys. Rev. B **30**, 1048 (1984).

[5] L. E. Klebanoff, S. W. Robey, G. Liu, and D. A. Shirley, Phys. Rev. B **31**, 6379 (1985).

[6] L. E. Klebanoff, R. H. Victora, L. M. Falicov, and D. A. Shirley, Phys. Rev. B **32**, 1997 (1985).

[7] J. A. Stroscio, D. T. Pierce, A. Davies, R. J. Celotta, and M. Weinert, Phys. Rev. Lett. **75**, 2960 (1995).

[8] E. Fawcett, Rev. Mod. Phys. **60**, 209 (1988).

[9] P. Habibi, C. Barreteau, and A. Smogunov, J. Phys.: Condens. Matter **25**, 146002 (2013).

[10] O. Y. Kolesnychenko, R. de Kort, M. I. Katsnelson, A. I. Lichtenstein, and H. van Kempen, Nature (London) **415**, 507 (2002).

[11] O. Y. Kolesnychenko, G. M. M. Heijnen, A. K. Zhuravlev, R. de Kort, M. I. Katsnelson, A. I. Lichtenstein, and H. van Kempen, Phys. Rev. B **72**, 085456 (2005).

[12] T. Hänke, M. Bode, S. Krause, L. Berbil-Bautista, and R. Wiesendanger, Phys. Rev. B **72**, 085453 (2005).

[13] M. Budke, T. Allmers, M. Donath, and M. Bode, Phys. Rev. B **77**, 233409 (2008).

[14] G. Adhikary, R. Bindu, S. Patil, and K. Maiti, Appl. Phys. Lett. **100**, 042401 (2012).

[15] M. Schüler, S. Barthel, M. Karolak, A. I. Poteryaev, A. I. Lichtenstein, M. I. Katsnelson, G. Sangiovanni, and T. O. Wehling, Phys. Rev. B **93**, 195115 (2016).

[16] L. Peters, D. Jacob, M. Karolak, A. I. Lichtenstein, and M. I. Katsnelson, Phys. Rev. B **96**, 245137 (2017).

[17] J. Kroha and P. Wölfle, J. Phys. Soc. Jpn. **74**, 16 (2005).

[18] S. Baroni, P. Giannozzi, and A. Testa, Phys. Rev. Lett. **58**, 1861 (1987).

[19] S. Baroni, S. de Gironcoli, A. Dal Corso, and P. Giannozzi, Rev. Mod. Phys. **73**, 515 (2001).

[20] M. Wierzbowska, S. de Gironcoli, and P. Giannozzi, arXiv:cond-mat/0504077.

[21] S. D. Brorson, A. Kazeroonian, J. S. Moodera, D. W. Face, T. K. Cheng, E. P. Ippen, M. S. Dresselhaus, and G. Dresselhaus, Phys. Rev. Lett. **64**, 2172 (1990).

[22] W. L. McMillan, Phys. Rev. **167**, 331 (1968).

[23] P. Hohenberg and W. Kohn, Phys. Rev. **136**, B864 (1964).

[24] W. Kohn and L. J. Sham, Phys. Rev. **140**, A1133 (1965).

[25] J. P. Perdew, *Electronic Structure of Solids* (Akademie Verlag, Berlin, 1991).

[26] J. P. Perdew and Y. Wang, Phys. Rev. B **45**, 13244 (1992).

[27] J. P. Perdew, K. Burke, and M. Ernzerhof, Phys. Rev. Lett. **77**, 3865 (1996).

[28] P. Giannozzi, S. Baroni, N. Bonini, M. Calandra, R. Car, C. Cavazzoni, D. Ceresoli, G. L. Chiarotti, M. Cococcioni, I. Dabo *et al.*, J. Phys. Condens. Matter **21**, 395502 (2009).

[29] P. Giannozzi, O. Andreussi, T. Brumme, O. Bunau, M. Buongiorno Nardelli, M. Calandra, R. Car, C. Cavazzoni, D. Ceresoli, M. Cococcioni *et al.*, J. Phys. Condens. Matter **29**, 465901 (2017).

[30] G. B. Bachelet, D. R. Hamann, and M. Schlüter, Phys. Rev. B **26**, 4199 (1982).

[31] D. M. Bylander and L. Kleinman, Phys. Rev. B **43**, 12070 (1991).

[32] A. Dal Corso, Phys. Rev. B **64**, 235118 (2001).

[33] R. Soulairol, C.-C. Fu, and C. Barreteau, J. Phys. Condens. Matter **22**, 295502 (2010).

[34] A. Rehbein, D. Wegner, G. Kaindl, and A. Bauer, Phys. Rev. B **67**, 033403 (2003).

[35] D. Tabor, J. M. Wilson, and T. J. Bastow, Surface Sci. **26**, 471 (1971).

[36] D. P. Jackson, Surface Sci. **43**, 431 (1974).

[37] A. C. Hewson, J. Phys. C **14**, 2747 (1981).